The Astrophysical Journal Supplement Series, 235:2 (8pp), 2018 March https://doi.org/10.3847/1538-4365/aaa5b3

Dielectronic and Trielectronic Recombination Rate Coefficients of Be-like Ar^{14+}

Z. K. Huang[1], W. Q. Wen[1], X. Xu[2], S. Mahmood[1], S. X. Wang[2], H. B. Wang[1], L. J. Dou[1], N. Khan[1,3], N. R. Badnell[4], S. P. Preval[4], S. Schippers[5], T. H. Xu[6], Y. Yang[6], K. Yao[6], W. Q. Xu[7], X. Y. Chuai[1], X. L. Zhu[1], D. M. Zhao[1], L. J. Mao[1], X. M. Ma[1], J. Li[1], R. S. Mao[1], Y. J. Yuan[1], B. Wu[1], L. N. Sheng[1], J. C. Yang[1], H. S. Xu[1], L. F. Zhu[2], and X. Ma[1]
[1] Institute of Modern Physics, Chinese Academy of Sciences, 730000, Lanzhou, People's Republic of China; wenweiqiang@impcas.ac.cn, x.ma@impcas.ac.cn
[2] Hefei National Laboratory for Physical Sciences at Microscale, Department of Modern Physics, University of Science and Technology of China, 230026, Hefei, People's Republic of China
[3] University of Chinese Academy of Sciences, 100049, Beijing, People's Republic of China
[4] Department of Physics, University of Strathclyde, Glasgow G4 0NG, UK
[5] I. Physikalisches Institut, Justus-Liebig-Universität Gießen, D-35392 Giessen, Germany
[6] Institute of Modern Physics, Fudan University, 200433, Shanghai, People's Republic of China
[7] Department of Mathematics and Physics, Bengbu University, 233000, Bengbu, People's Republic of China
Received 2017 November 24; revised 2018 January 2; accepted 2018 January 4; published 2018 February 21

Abstract

Electron–ion recombination of Be-like $^{40}Ar^{14+}$ has been measured by employing the electron–ion merged-beams method at the cooler storage ring CSRm. The measured absolute recombination rate coefficients for collision energies from 0 to 60 eV are presented, covering all dielectronic recombination (DR) resonances associated with $2s^2 \rightarrow 2s2p$ core transitions. In addition, strong trielectronic recombination (TR) resonances associated with $2s^2 \rightarrow 2p^2$ core transitions were observed. Both DR and TR processes lead to series of peaks in the measured recombination spectrum, which have been identified by the Rydberg formula. Theoretical calculations of recombination rate coefficients were performed using the state-of-the-art multi-configuration Breit–Pauli atomic structure code AUTOSTRUCTURE to compare with the experimental results. The plasma rate coefficients for DR +TR of Ar^{14+} were deduced from the measured electron–ion recombination rate coefficients in the temperature range from 10^3 to 10^7 K, and compared with calculated data from the literature. The experimentally derived plasma rate coefficients are 60% larger and 30% lower than the previously recommended atomic data for the temperature ranges of photoionized plasmas and collisionally ionized plasmas, respectively. However, good agreement was found between experimental results and the calculations by Gu and Colgan et al. The plasma rate coefficients deduced from experiment and calculated by the current AUTOSTRUCTURE code show agreement that is better than 30% from 10^4 to 10^7 K. The present results constitute a set of benchmark data for use in astrophysical modeling.

Key words: atomic data – atomic processes – plasmas

1. Introduction

It has been estimated that more than 90% of the visible matter in the universe is in the plasma state (Müller 2008). Astrophysical plasmas can be divided into two main classes, (i) the collisionally ionized plasma formed in stars, supernova remnants, and galaxies, and (ii) photoionized plasmas formed in sources such as planetary nebulae, X-ray binaries, and active galactic nuclei. Various types of reactions take place in astrophysical plasmas, such as electron collision excitation, electron impact ionization, and electron–ion recombination (Savin 2007). Emission features originating from these plasmas are essential for deducing the properties of the plasmas, such as temperature, density, and elemental abundances (Beiersdorfer 2003; Kallman & Palmeri 2007). Electron–ion recombination processes such as radiative recombination (RR) and dielectronic recombination (DR) contribute substantially to the line emission for photoionized plasmas. In addition, the ionization balance of a plasma is determined by the relative rates of ionization and recombination.

In order to understand astrophysical plasmas, space-based observatories, such as *Chandra* and *XMM-Newton*, have been launched to observe X-ray emission from various astrophysical objects (Paerels & Kahn 2003). All the observed emission and absorption lines have to be explained by plasma modeling, and most of the input atomic data for these plasma models are from theory. However, many theories cannot calculate the DR rate coefficients with sufficient precision and have large uncertainties, especially at low energies, due to sensitivity in the positioning of resonances. As a result, precise electron–ion recombination data from experiments are required to explain the astrophysical observations and to benchmark the theory. With these data, information pertaining to these astrophysical objects, such as the structure, elemental composition, energy balance, and temperature distribution, can be investigated (Kallman & Palmeri 2007).

The importance of DR in a plasma was recognized for the first time by Burgess in 1964 (Burgess 1964). Since then, DR has been considered an important process in atomic physics and plasma physics. DR experiments on highly charged ions employing the electron–ion merged-beams technique have been developed for more than two decades at heavy ion storage rings, i.e., the TSR at MPIK in Heidelberg (Schippers 2015), the ESR at GSI in Darmstadt (Brandau & Kozhuharov 2012), Germany, and the CRYRING at MSL in Stockholm, Sweden (Schuch & Böhm 2007). The main cooler storage ring (CSRm), equipped with an electron cooler, provides an ideal research platform for electron–ion recombination experiments of highly charged ions at the heavy ion research facility in Lanzhou (Huang et al. 2017). More details about DR experiments at storage rings can be found in the recent reviews of Brandau & Kozhuharov (2012), Brandau et al. (2015), Müller (2008), and

Schippers (2015), and in the references cited therein. Recent reviews of experimental DR measurements for astrophysics applications were given by Schippers (2012).

Argon is one of the most abundant heavy elements in the universe and also in the solar system. The emission lines from argon have already been observed and were used for plasma diagnostics (Dere et al. 2001). In addition, Be-like argon has been observed in hot solar plasmas where the temperature is $\sim 10^6$ K (Bhatia & Landi 2008). The intensity ratios of the emission lines from Ar^{14+} were used to diagnose coronal plasmas (Landi et al. 2001; Saloman 2010). Therefore, investigating the recombination of Be-like Ar will provide very useful astrophysical information. Note that the emission lines from highly charged argon have been investigated at an electron beam ion trap (EBIT; Träbert et al. 2000; Lepson et al. 2003). Here, we present absolute rate coefficients for electron–ion recombination of Be-like argon from an experiment at the main cooler storage ring CSRm and from theoretical calculations using the AUTOSTRUCTURE code.

For Be-like Ar^{14+}, the experimental electron–ion collision energy range was 0–60 eV. The most significant recombination channels in this energy range are

$$\mathrm{Ar}^{14+}(2s^2\ {}^1S_0) + e^- \rightarrow \left\{ \begin{array}{l} \mathrm{Ar}^{13+}[2s^2 nl],\ \mathrm{RR}; \\ \mathrm{Ar}^{13+}[2s2p({}^3P_{0,1,2})nl],\ n \geqslant 10,\ \mathrm{DR}; \\ \mathrm{Ar}^{13+}[2s2p({}^1P_1)nl],\ n \geqslant 7,\ \mathrm{DR}; \\ \mathrm{Ar}^{13+}[2p^2({}^3P_{0,1,2};\ {}^1D_2;\ {}^1S_0)nl],\ n \geqslant 6,\ \mathrm{TR}; \end{array} \right\}, \quad (1)$$

where RR, DR, and TR denote radiative, dielectronic, and trielectronic recombination, respectively. In RR, a free electron is captured into a bound state of the ion and a photon is emitted. DR is a two-step process: a doubly excited intermediate state is formed through a resonant process involving capture of a free electron and simultaneous excitation of a bound electron, then the doubly excited state decays via photon emission such that the charge state of the recombined ion is stabilized. In the case of TR, the capture is associated with the excitation of two core electrons to higher levels, and completed when the triply excited intermediate level decays by photon emission. The excitation energies of the core electrons and lifetimes associated with $\Delta N = 0$ (here N is the principal quantum number of the transition core electron) DR and TR are listed in Table 1.

Storage ring electron–ion recombination experiments have been performed on a number of Be-like ions, with emphases on different physical topics. Astrophysical data needs were specifically addressed with DR studies of C^{2+}, N^{3+}, O^{4+} (Fogle et al. 2005), F^{5+} (Ali et al. 2013), Ne^{6+} (Orban et al. 2008), Mg^{8+}, (Schippers et al. 2004), Si^{10+} (Orban et al. 2010; Bernhardt et al. 2016), and Fe^{22+} (Savin et al. 2006). Other topics were trielectronic recombination of Cl^{13+} (Schnell et al. 2003) and hyperfine-induced transition rate measurements with Ti^{18+} (Schippers et al. 2007) and S^{12+} (Schippers et al. 2012). In addition, the Be-like ions Ge^{28+} (Orlov et al. 2009) and Xe^{50+} (Bernhardt et al. 2015) were employed to test QED and electron–electron correlation effects. It is noted that the significance of TR was first observed for Be-like Cl^{13+} (Schnell et al. 2003) and subsequently confirmed for several ions from this isoelectronic sequence. For Be-like Mg, a distinct contribution from TR in the form of several sharp peaks was also found (Schippers et al. 2004). Toward higher Z ions, some TR resonance features appear in the recombination spectrum of Ti^{18+} (Schippers et al. 2007), whereas in case of Fe^{22+} only one clear peak could be attributed to TR (Savin et al. 2006).

Here, we report the first measurement of the electron–ion recombination spectrum of Be-like Ar. The paper is structured as follows. The experimental method and the data analysis are presented in Section 2. In Section 3, we give a brief description of the theoretical method used by AUTOSTRUCTURE. In Section 4, the experimental results, including merged-beam DR rate coefficients, and also plasma rate coefficients, are presented and compared to currently available results in the literature. A conclusion is given in Section 5.

Table 1
Excitation Energies and Lifetimes for $\Delta N = 0$ of Be-like Ar^{14+} Levels

Level	Energy		Lifetime
	NIST (eV)	(Wang et al. 2015)	
	(eV)	(eV)	(s)
$1s^2\ 2s^2\ {}^1S_0$	0.00000	0.00000	∞
$1s^2\ 2s2p\ {}^3P_0$	28.3530	28.3604	4.2[6][a]
$1s^2\ 2s2p\ {}^3P_1$	29.2429	29.2509	3.436[−07]
$1s^2\ 2s2p\ {}^3P_2$	31.3283	31.3383	1.543[−02]
$1s^2\ 2s2p\ {}^1P_1$	56.0630	56.0704	1.070[−10]
$1s^2\ 2p^2\ {}^3P_0$	75.0000	75.0125	1.432[−10]
$1s^2\ 2p^2\ {}^3P_1$	76.2776	76.2740	1.369[−10]
$1s^2\ 2p^2\ {}^3P_2$	77.9000	77.9070	1.345[−10]
$1s^2\ 2p^2\ {}^1D_2$	⋯	85.4889	4.789[−10]
$1s^2\ 2p^2\ {}^1S_0$	104.224	104.196	6.9199[−11]

Note. Numbers in brackets denote powers of 10. The data cited from NIST are from the Kramida et al. (2015).
[a] Lifetime associated with the E1M1 two-photon transition taken from Fritzsche et al. (2015).

2. Experiment and Data Analysis

Measurements were performed at the main cooler storage ring (CSRm) at the Institute of Modern Physics in Lanzhou, China. A detailed description of the experimental setup and method for DR experiments at the CSRm has already been given in the literature (Huang et al. 2015, 2017). Here, we will only briefly describe the electron–ion recombination experiment with Be-like Ar^{14+}at the CSRm.

In the experiment $^{40}Ar^{14+}$ ions were produced from an Electron Cyclotron Resonance (ECR) ion source (Zhao et al. 2017) and accelerated to a beam energy of 6.928 MeV/u by a Sector Focused Cyclotron, and then were injected into the CSRm. The stored ion current was typically $\sim 50\ \mu$A. The beam lifetime was about 50 s. The electron cooler at the CSRm was employed to cool the ion beam, and was also used as an electron target in the measurement. During the experiment, the ion beam was merged with the electron beam over an effective interaction length of $L = 4.0$ m in the cooler section. The electron beam was adiabatically expanded from the magnetic field of 125 mT at the electron-gun section to 39 mT at the electron-cooling section, thus a colder electron beam was generated and a higher experimental resolution could

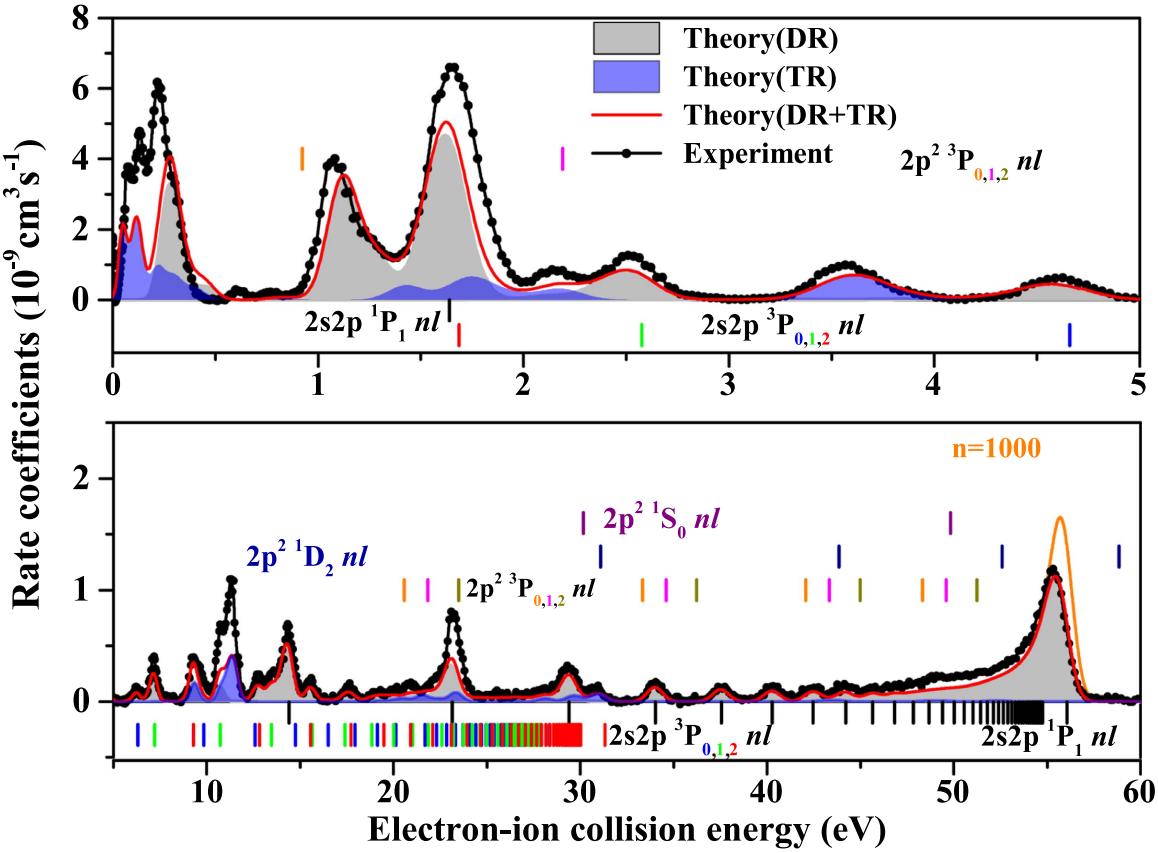

Figure 1. Electron–ion recombination rate coefficients of Be-like argon as a function of relative collision energy. The energy scale of the experimental spectrum (connected filled circles) was recalibrated by a factor of 1.06 to achieve agreement with the known $2s2p\ (^1P_1)\ nl$ series limit at 56.063 eV. Four $\Delta N = 0$ DR series associated with $2s^2 \rightarrow 2s2p$, $^1P_1$, $^3P_{0,1,2}$ core excitations and parts of five $\Delta N = 0$ TR series ($2s^2 \rightarrow 2p^2$, $^1S_0$, $^1D_2$, $^3P_{0,1,2}$) can be observed. The corresponding resonance positions are indicated by short bars in different colors. The calculated DR and TR rate coefficients are shown by the gray area and the blue area, respectively. The sum of the theoretical DR and TR contribution is shown as a solid red line. This curve accounts for the experimental field-ionization cutoff (see the text). The orange line from 45 eV to 60 eV is the theoretical result including the full DR resonance strength up to $n_{\max} = 1000$, called the field-ionization-free recombination rate coefficient.

be realized. The diameter of the electron beam was measured to be ~50 mm at the cooling section, with typical electron densities being $n_e = 1.1 \times 10^6\,\mathrm{cm}^{-3}$.

During the measurement, the injected ion beam was first electron-cooled for several seconds in order to decrease the diameter and the momentum spread of the ion beam. Then, the electron energy detuning system added a bias voltage to the cathode voltage of the electron cooler to scan the electron beam energy according to a preset timing sequence (Meng et al. 2013). This provided a nonzero relative kinetic energy between electrons and ions. Downstream of the electron cooler, the recombined ions were separated from the primary ion beam in the first bending magnet and detected by a movable scintillator particle detector with nearly 100% efficiency (Wen et al. 2013). During the measurement, a DC current transformer was used to monitor the ion beam current in real time. Ion and electron beam position monitors were utilized to monitor the relative positions of the ion beam and the electron beam in the cooling section. All of the DR measurements were performed under the condition of keeping the electron beam and ion beam parallel along the axis of the cooler. In addition, a Schottky pick-up was employed to monitor the revolution frequency and the momentum spread of the ion beam, and to correct the experimental data in the offline data analysis (Wu et al. 2013).

In the DR experiments at heavy ion storage rings, the recombination rate coefficients α can be deduced from the background-subtracted recombination counting rate R at a relative energy E_{rel} between electron and ion by Bernhardt et al. (2011):

$$\alpha(E) = \frac{R}{N_i n_e (1 - \beta_e \beta_i)} \cdot \frac{C}{L}, \tag{2}$$

where N_i is the number of stored ions, n_e is the density of electron beam, $\beta_e = \upsilon_e/c$ and $\beta_i = \upsilon_{\mathrm{ion}}/c$ are the velocities of the electron beam and ion beam, L is the length of the effective interaction section, and C is the circumference of the storage ring.

3. Theory

For a better understanding of the measured electron–ion recombination spectrum, a theoretical calculation using the distorted-wave collision package AUTOSTRUCTURE (Badnell 2011) was performed to calculate recombination cross sections and rate coefficients. AUTOSTRUCTURE is a versatile code that is able to calculate energy levels, oscillator strengths, radiative/autoionization rates, and many other quantities using semi-relativistic kappa-averaged wavefunctions. The underlying theory implemented by AUTOSTRUCTURE for DR is well documented, however, we discuss it briefly here. For a target ion $X_\nu^{(Q)}$ with a residual charge Q, and initial state ν, colliding with an electron and recombining into

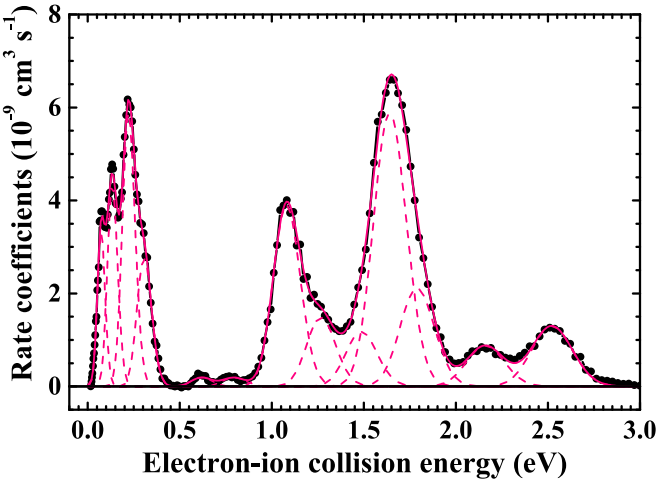

Figure 2. Peak fit (the solid pink line) to the experimental low-energy DR rate coefficient (black filled symbols). In the fit, 13 δ-like resonances were convoluted with a flattened Maxwellian electron energy distribution that is characterized by the temperatures $T_\parallel$ and $T_\perp$ in the longitudinal and transversal directions, respectively, with respect to the electron beam propagation direction. The fit resulted in $k_B T_\parallel = 2.40(6)$ meV and $k_B T_\parallel = 11.91(87)$ meV. The individual peaks are shown as dashed pink lines. The fitted resonance energies and strengths are given in Table 2.

an ion $X_f^{(Q-1)}$ with a final state f, the partial DR cross section σ_{fv}^{Q}, energy averaged over a bin width ΔE_c, can be expressed as

$$\sigma_{fv}^{Q}(E_c) = \frac{(2\pi a_0 I_H)^2 \tau_0}{E_c} \sum_j \frac{\omega_j}{2\omega_v} \frac{\sum_l A^a_{j\to v,E_c l} A^r_{j\to f}}{\sum_h A^r_{j\to h} + \sum_{m,l} A^a_{j\to m,E_c l}}, \quad (3)$$

where ω_v and ω_j are the statistical weights for the N-and $(N+1)$-electron states, respectively. The A^r and A^a are the radiative and autoionization rates, respectively, and E_c is the energy of the continuum electron with angular momentum l, fixed by the position of the resonances. I_H is the ionization energy of the hydrogen atom, k_B is the Boltzmann constant, and $(2\pi a_0)^2\tau_0 = 2.6741 \times 10^{-32}$ cm^2 s. The sum over l covers the angular momentum quantum numbers of the Rydberg electron. The sum over j covers all autoionization states. Lastly, the sum over h and m represents the total radiative and autoionization widths, respectively.

For the N-electron core configurations, we included $2s^2$, $2s2p$, and $2p^2$, and for the $(N+1)$ electron, we included $2s^22p$, $2s2p^2$, and $2p^3$. No promotions from $1s^2$ are included, hence they are omitted from the configuration list. For the recombined Rydberg electron, radiative/autoionization rates were calculated explicitly for principal quantum numbers $n = 3$ up to $n = 100$, after which the rates were calculated for quasi-logarithmically spaced values of n up to $n = 1000$. Interpolation was then used to obtain the remaining n. For each n, we calculated radiative/autoionization rates for sufficiently many angular momentum quantum numbers l so as to numerically converge the total DR rate coefficient to <1% over the temperature range Q^2(10–10^6) K.

In order to compare with the experimentally derived electron–ion recombination rate coefficients on the one hand and to calculate the plasma rate coefficient on the other hand, the calculated recombination cross section $\sigma(v)$ has to be convoluted with the appropriate electron-velocity distribution

Table 2
Results of the Peak Fits to the Experimental Merged-beams DR Rate Coefficient at Electron–Ion Collision Energies below 3 eV (see Figure 2)

Resonance energy (eV)	Resonance strength (10^{-18} cm^2 eV)
0.08269(84)	10.57(15)
0.14436(88)	13.32(15)
0.23232(94)	17.78(17)
0.3173(14)	8.25(17)
0.629(18)	0.57(12)
0.805(21)	0.56(12)
1.091(17)	11.51(17)
1.2786(63)	0.44(16)
1.450(18)	3.46(53)
1.6524(62)	17.27(41)
1.8005(85)	6.19(65)
2.1714(74)	2.58(12)
2.5327(52)	3.81(12)

Note. The numbers in parentheses denote the uncertainties obtained from the fit and correspond to one standard deviation.

to obtain the rate coefficients,

$$\alpha(E) = \langle v\sigma \rangle = \int v\sigma(v) f(v) d^3v, \quad (4)$$

where $f(v)$ is the electron-velocity distribution. For the case with the merged-beams rate coefficient, it is a flattened Maxwellian (Kilgus et al. 1992) that is characterized by the longitudinal and transverse temperatures $T_\parallel$ and $T_\perp$ with respect to the propagation direction of the electron beam. For the case with the plasma rate coefficient, $f(v)$ is an isotropic Maxwellian characterized by the electron temperature T_e of the plasma.

4. Results and Discussion

4.1. Merged-beams DR Rate Coefficients

The DR spectra of Be-like $^{40}Ar^{14+}$ obtained from the DR experiment at the CSRm and from the AUTOSTRUCTURE calculations are compared and shown in Figure 1. The measured spectrum covers the whole energy range of DR resonances associated with $2s \to 2p(\Delta N = 0)$ core excitations. In the recombination spectrum, the resonance positions of each Rydberg state can be well-approximated by the Rydberg formula:

$$E_{res} = E_{exc} - I_H\left(\frac{Q}{n}\right)^2, \quad (5)$$

where E_{exc} is the core excitation energy of the ions, which is taken from the NIST database, I_H is the ionization energy of the hydrogen atom, and Q is the charge state of the target ion. The associated Rydberg resonance series of the doubly excited intermediate levels $2s2p(^1P_1)nl$ and $2s2p(^3P_J)nl$ are indicated by vertical bars. In Figure 1 the experimental energy scale was recalibrated by a factor of 1.06 to achieve agreement with the known $2s2p(^1P_1)nl$ series limit at 56.063 eV. As shown in Figure 2, by fitting each of the first 13 resonance peaks at relative energy below 0.5 eV with a flattened Maxwellian function (Kilgus et al. 1992), the longitudinal and transversal electron temperatures were obtained, yielding $k_B T_\parallel = 2.40(6)$ meV and $k_B T_\perp = 11.91(87)$ meV, respectively. The peak fit results are

listed in Table 2. The numbers in parentheses denote the uncertainties obtained from the fit and correspond to one standard deviation. From the fit, it is concluded that the experimental energy resolution is less than 0.07 eV FWHM at relative energies around 0.2 eV.

In the experiment, the recombined ions have to travel through a toroidal magnet, three quadrupole magnets, and a dipole magnet before their detection. The electric field arising from these magnetic fields can ionize the recombined ions in high-n Rydberg levels. As a result, the ions recombining into states with the outer electron having a principal quantum number $n > n_{\rm cutoff}$ will be field-ionized in the separating dipole magnet and cannot be detected. The critical quantum number $n_{\rm cutoff}$ for field ionization of an ion in a magnetic field can be estimated from the formula (Fogle et al. 2005)

$$n_{\rm cutoff} \simeq \left(6.2 \times 10^8 V/{\rm cm}\frac{Q^3}{\upsilon_i B}\right)^{1/4}, \quad (6)$$

where Q is the charge state of the ion, υ_i is the ion velocity, and B is the magnetic field strength. In the present experiment the estimated cutoff quantum number in the charge-separating dipole magnet is $n_{\rm cutoff} = 74$. The field-ionization effect can be seen at the series limits of $2s2p(^1P_1)nl$ around 55 eV in Figure 1. Compared with the $2s2p\ (^1P_1)nl$ series, the $2s2p(^3P_J)nl$ series limits were not observed in the DR spectra.

To fully understand the measured electron–ion recombination rate coefficients, a convolution of the calculated DR resonance cross sections with the velocity distribution of the electron beam was performed by AUTOSTRUCTURE, as described in Section 3. The gray area shows the theoretical DR rate coefficients, taking field ionization into account. It turns out that the resonance peaks around 0.5, 4, and 11 eV cannot be fully identified by considering only the $2s2p(^1P_1)nl$ and $2s2p(^3P_J)nl$ DR series (Figure 1). These peaks can be attributed to TR-associated $2s^2 \rightarrow 2p^2$ ($^1S_0$, $^1D_2$, $^3P_{0,1,2}$) core double-excitations, as revealed by a separate calculation of TR contributions. The calculated TR rate coefficients are shown as the blue shaded area in Figure 1. The sum of the calculated DR and TR rate coefficients is shown as a solid red line. This curve accounts for field ionization, i.e., it contains a contribution of recombination resonance from Rydberg levels up to 150 by taking into account time-of-flight survival probabilities for n, as described in Schippers et al. (2001). An additional calculation including DR and TR contributions from capture into Rydberg states up to $n_{\rm max} = 1000$ from 45 to 60 eV is shown in Figure 1 as a solid orange line, and is known as the field-ionization-free electron–ion recombination rate coefficient. Agreement between the calculated results and experimental rate coefficients was found to be better than 30% for the whole energy range. However, there is a discrepancy in the resonance positions and intensity at energies less than 0.5 eV. This is due to electron–electron correlation effects. The intensity of resonances at 11 eV and 23 eV is also not well-produced by AUTOSTRUCTURE.

Note that Be-like ions are known to have long-lived $2s2p\ ^3P_J$ levels ($J = 0, 1, 2$), which might be present in the ion beams used for the experiment. For a Be-like $^{40}Ar^{14+}$ ion that has zero nuclear spin, the lifetimes of energy levels of $2s2p(^3P_1)$ and $2s2p(^3P_2)$ are very short (as listed in Table 1) and these two metastable levels will not survive, as the measurements were performed after several seconds of electron-cooling. However,

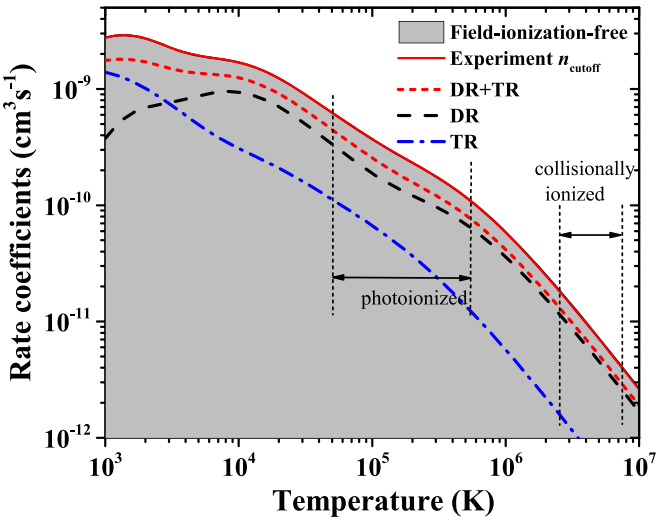

Figure 3. Plasma rate coefficients of Be-like Ar^{14+} as a function of the electron temperature. The solid red line is the experimentally derived $\Delta N = 0$ DR and TR rate coefficients. The theoretical results deduced from the AUTOSTRUCTURE code for $\Delta N = 0$ DR and for TR are shown as a dotted black line and a dashed–dotted blue line, respectively. The calculated sum of DR and TR is shown as a short-dashed red line. The experimentally derived field-ionization-free plasma rate coefficient is shown as a gray area. The approximate temperature ranges where Ar^{14+} is expected to form in photoionized plasmas and collisionally ionized plasmas are indicated by vertical dashed bars and associated arrows (Kallman & Bautista 2001; Bryans et al. 2009).

the lifetime of metastable level $^3P_0$ is very long and can only decay by a E1M1 two-photon transition. As a result, ions in the metastable state of $^3P_0$ are expected to have been present in the ion beam during the experiment. In order to determine the rate coefficient for the ground level of the ion, the contribution from the metastable level should be considered. However, in the case of Be-like Ar^{14+} there is an unknown fraction of metastable ions in the primary beam. As described in Orban et al. (2008), ion beams extracted from ECR ion sources showed a decreasing percentage of metastable content with increasing charge along the Be-like isoelectronic sequence. The metastable contents amount to 60%, 40%, 35%, 14%, and 10% for C^{2+}, N^{3+}, O^{4+}, Ne^{5+}, and Si^{10+} ion beams, respectively (Orban et al. 2008, 2010). Since we have also used an ECR ion source in this experiment, we estimated that the maximum metastable contents amount to 5% in the case of Be-like Ar^{14+} in our experiment. In addition, a separate calculation of electron–ion recombination for $2s2p(^3P_0)$ metastable ions by AUTOSTRUCTURE was performed. In the range of the $\Delta N = 0$ DR resonances, the calculation showed very weak metastable DR resonant strengths and its contribution can be safely neglected. However, at high temperatures the metastable contribution to the plasma rate coefficient becomes comparable with that from the ground, because of the strong $2p$–$3d$ promotion.

The uncertainty of the experimental recombination rate coefficients is estimated to be about 30% (at a 1σ confidence level), including a 5% uncertainty of the estimated metastable content of the Ar^{14+} ions, an uncertainty of 15% due to a combination of counting statistics, electron and ion beam currents, and interaction length, and an uncertainty of 20% due to the electron density distribution profile and also the position of the ion beam in this profile.

Table 3
Fitted Coefficients for the RR-subtracted $\Delta N = 0$ DR+TR Rate Coefficients from Figure 3 for Two Different Values of $n_{\rm cutoff}$ and $n_{\rm max} = 1000$ (Field-ionization-free)

No.	$n_{\rm cutoff}$		$n_{\rm max} = 1000$	
i	c_i	E_i	c_i	E_i
1	0.254	0.12	0.244	0.115
2	0.580	0.28	0.590	0.278
3	3.74	3.47	3.77	3.45
4	5.17	1.43	5.14	1.43
5	14.3	12.42	14.38	12.45
6	23.39	31.84	23.13	31.95
7	38.84	56.39	40.30	57.03

Note. The units of c_i and E_i are 10^{-3} cm^3 s^{-1} K$^{3/2}$ and eV, respectively.

4.2. Plasma Recombination Rate Coefficients

As mentioned above, storage ring measured electron–ion recombination rate coefficients are different from the plasma rate coefficients that were used for astrophysics modeling. In contrast to the very narrow velocity spread of the electron beam in a storage ring experiment, the electrons in astrophysical plasmas have a much broader and isotropic Maxwellian velocity spread. Therefore, the plasma rate coefficient can be obtained by convoluting the DR cross section $\sigma(E)$ with a Maxwell–Boltzmann distribution characterized by the plasma electron temperature T_e (see Equation (4), with $E = m_e v^2/2$ and electron rest mass m_e). At electron–ion energies $E \gg k_B T_\perp$ the DR cross section $\sigma(E)$ can be obtained as $\alpha(E)/v$, where $\alpha(E)$ denotes the measured merged-beams rate coefficient. At lower energies the influence of the experimental energy spread becomes noticeable, and consequently a different approach for the derivation of the plasma rate coefficient has to be applied. Here, this relates to the four lowest-energy resonances from Table 2. In particular, the lowest-energy resonance appears at an energy lower than $k_B T_\perp$. For these resonances, the DR cross section as obtained from the peak fit was used in the convolution procedure following the procedure laid out by Schippers et al. (2004).

The experimentally derived and theoretically calculated plasma rate coefficients as a function of electron temperature are shown in Figure 3 as the solid red line and the short-dashed red line, respectively. Both lines account for the field-ionization effect discussed above. The theoretically calculated DR and TR contributions are shown in Figure 3 by the black dashed line and the blue dotted–dashed line, respectively. In order to compare the experimental result to different theoretical models, the experimental recombination rate coefficient from 45 to 60 eV was replaced by the AUTOSTRUCTURE calculation including recombination into states up to $n_{\rm max} = 1000$ (the solid orange line in Figure 1). Such a derived field-ionization-free plasma rate coefficient is shown as a gray shaded area in Figure 3. It should be noted that the contribution from recombination into resonance levels with $n > 1000$ was considered very small and can be safely neglected.

The temperature range is from 10^3 to 10^7 K in Figure 3. It includes the ranges of photoionized and collisionally ionized plasmas for Be-like Ar. The boundaries of these temperature ranges are displayed by vertical dashed bars. These mark the temperatures where the fractional abundance of Be-like Ar is 10% of its maximum value (Kallman & Bautista 2001; Bryans et al. 2009). At a temperature of 10^3 K the TR contribution is a factor of four larger than the DR contribution. In the temperature range of photoionized plasmas, the TR contribution to the total plasma rate coefficient amounts to 10%. Finally, an agreement of better than 30% for the whole temperature range is found between the present experimentally derived rate coefficients and the current AUTOSTRUCTURE calculations.

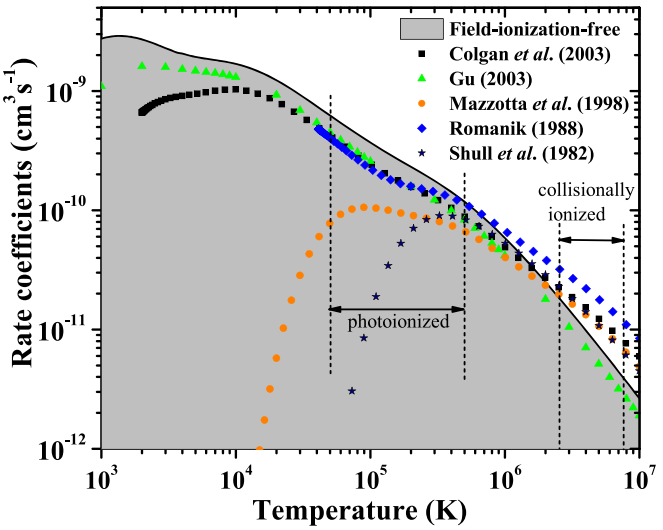

Figure 4. Comparison of field-ionization-free resonant plasma recombination rate coefficients with theoretical calculated results for Be-like Ar. Full squares show rate coefficients by Colgan et al. (2003). Calculations by Gu (2003) and Mazzotta et al. (1998) are shown by full triangles and full circles, respectively. Rate coefficients of Romanik (1988) and Shull & Van Steenberg (1982) are shown by full diamonds and stars, respectively. Temperature ranges where the Be-like Ar concentration is higher than 10% of its maximum abundance in photoionized and collisionally ionized plasmas are shown by vertical dashed bars, as in Figure 3 (Kallman & Bautista 2001; Bryans et al. 2009).

In order to compare with other recommended theoretical data in the literature and to make convenient use of the presently measured results in plasma modeling, the $\Delta N = 0$ resonant plasma rate coefficients were fitted with the function

$$\alpha(T_e) = T_e^{-3/2} \sum_i c_i \times \exp\left(-\frac{E_i}{kT_e}\right). \quad (7)$$

The fit parameters of c_i and E_i are listed in Table 3, and reproduce the data within 2% at $\sim 10^3$ K and better than 1% up to 10^7 K.

In Figure 4, the experimentally derived field-ionization-free plasma rate coefficients including DR and TR are compared with the theoretical data from the literature. The temperature ranges where Ar^{14+} forms in collisionally ionized plasmas and photoionized plasmas are indicated by vertical dashed bars, just as shown in Figure 3. Among the literature data, only the theoretical calculations from Colgan et al. (2003) and Gu (2003) provide plasma rate coefficients at low temperatures. The calculations of Colgan et al. (2003) used AUTOSTRUCTURE and Gu (2003) used FAC code. Note that the plot of Colgan et al. (2003) as shown in Figure 4 is fitted by using the revised fit on the ADAS website (Badnell 2009). The other calculations yielded plasma rate coefficients only at temperatures higher than 10^4 K.

At a temperature of 10^4 K, the calculated plasma rate coefficients from Colgan et al. (2003) and Gu (2003) are 30% lower than those of the experimental data. In the temperature range around 2×10^5 K, where Be-like Ar is expected to be

abundant in photonionized plasmas, the calculated plasma rate coefficients from Colgan et al. (2003), Gu (2003), and Romanik (1988)) are 30% lower than the experimental results, and the data from Mazzotta et al. (1998) and Shull & Van Steenberg (1982) are about 60% lower than the results of experimental data.

At a temperature of about 3×10^6 K, where Ar^{14+} is supposed to be abundant in collisionally ionized plasmas, the theoretical data of Gu (2003) are 25% lower than the data of the experimental results. The calculated data from Colgan et al. (2003), Mazzotta et al. (1998), Romanik (1988), and Shull & Van Steenberg (1982) are 30%, 15%, 80%, and 30% higher than the experimental data. Above 6×10^6 K, the calculation of Gu (2003) is about 25% lower than the experimental data, but the calculations of Colgan et al. (2003), Mazzotta et al. (1998), Romanik (1988), and Shull & Van Steenberg (1982) are all more than 30% higher than the experimental data. Note that the calculation of Gu (2003) shown in Figure 4 only included transitions for $\Delta N = 0$, and the data from Colgan et al. (2003), Mazzotta et al. (1998), Romanik (1988), and Shull & Van Steenberg (1982) shown in Figure 4 included the transitions for $\Delta N = 0$ and $\Delta N = 1$. As a result, DR through excitation of the $2s$ electron to higher shells ($\Delta N > 0$ DR) and also through excitation of a $1s$ electron, which is not included in the experimental data, could be the reason for this discrepancy. Note that greater than 2% between the current calculation by the AUTOSTRUCTURE code (as shown in Figure 3 as a short-dashed red line) and the data from Colgan et al. (2003) is found if only taking into account of $\Delta N = 0$ core electron excitation. In summary, agreement within about 35% was found between experimentally derived plasma rate coefficients and theoretical calculations by Colgan et al. (2003) and Gu (2003) in the temperature range from 10^4 to 10^7 K.

5. Conclusions

Electron–ion recombination rate coefficients of Be-like Ar^{14+} forming into B-like Ar^{13+} were derived from a measurement performed by employing the electron–ion merged-beams method at the cooler storage ring CSRm. No previous experimental results were available for this ion. The resonances associated with dielectronic ($2s^2 \rightarrow 2s2p$) and trielectronic ($2s^2 \rightarrow 2p^2$) $\Delta N = 0$ recombination within the energy range of 0–60 eV were investigated and identified by application of the Rydberg formula. Agreement in terms of DR resonance positions and strengths was found to be better than 10% and 30%, respectively, between the experimental recombination rate coefficient and the newly calculated results using the distorted-wave code AUTOSTRUCTURE. The TR resonance positions and strengths were also reproduced by the AUTOSTRUCTURE calculation.

For use in plasma modeling, the plasma recombination rates coefficient was deduced from the merged-beams recombination rate coefficients. The temperature range of this plasma rate coefficient is from 10^3 to 10^7 K. This range comprises the temperatures where the ions are abundant both in photoionized and collisionally ionized plasmas. The experimentally derived plasma rate coefficient was compared with the calculated data from existing literature. At the temperature range of photoionized plasmas, the experimentally derived rate coefficient is still up to 30% larger than the more recent results of (Gu 2003), (Romanik 1988) and (Colgan et al. 2003). For temperatures higher than 10^6 K, the experimentally derived plasma rate coefficients are lower than the calculated data from the literature except for Gu (2003), which only showed $\Delta N = 0$ core electron excitation. Agreement of better than 30% for the whole temperature range was found between the present experimentally derived plasma rate coefficients and the calculated results from AUTOSTRUCTURE. Our data thus provide a stringent benchmark for Ar^{14+} recombination data used in astrophysical modeling.

This work is partly supported by the National Key R&D Program of China under grant No. 2017YFA0402300, the National Natural Science Foundation of China through No. 11320101003, No. 91336102, No. U1732133, No. 11611530684, the Strategic Priority Research Program of the Chinese Academy of Sciences, grant No. XDB21030900 and the Key Research Program of Frontier Sciences, CAS, grant No. QYZDY-SSW-SLH006. W. Wen acknowledges the support by the Youth Innovation Promotion Association of the Chinese Academy of Sciences. S.P. Preval and N.R. Badnell acknowledge the support of EPSRC grant EP/L021803/1. S. Schippers gratefully acknowledges support by the CAS President's International Fellowship Initiative (PIFI). A helpful discussion with R. Schuch is acknowledged. The authors would like to thank the crew of the Accelerator Department for skillful operation of the CSR accelerator complex.

ORCID iDs

W. Q. Wen https://orcid.org/0000-0001-5266-3058
S. Schippers https://orcid.org/0000-0002-6166-7138
L. F. Zhu https://orcid.org/0000-0002-5771-0471
X. Ma https://orcid.org/0000-0001-9831-0565

References

Ali, S., Orban, I., Mahmood, S., Loch, S. D., & Schuch, R. 2013, A&A, 557, A2
Badnell, N. R. 2009, Atomic and Molecular Diagnostic Processes in Plasmas
Badnell, N. R. 2011, CoPhC, 182, 1528
Beiersdorfer, P. 2003, ARA&A, 41, 343
Bernhardt, D., Becker, A., Brandau, C., et al. 2016, JPhB, 49, 074004
Bernhardt, D., Brandau, C., Harman, Z., et al. 2011, PhRvA, 83, 020701
Bernhardt, D., Brandau, C., Harman, Z., et al. 2015, JPhB, 48, 144008
Bhatia, A. K., & Landi, E. 2008, ADNDT, 94, 223
Brandau, C., & Kozhuharov, C. 2012, in Atomic Processes in Basic and Applied Physics, 283 ed. V. Shevelko & H. Tawara (Berlin: Springer), 283
Brandau, C., Kozhuharov, C., Lestinsky, M., et al. 2015, PhyS, 2015, 014022
Bryans, P., Landi, E., & Savin, D. W. 2009, ApJ, 691, 1540
Burgess, A. 1964, ApJ, 139, 776
Colgan, J., Pindzola, M. S., Whiteford, A. D., & Badnell, N. R. 2003, A&A, 412, 597
Dere, K., Landi, E., Young, P., & Del Zanna, G. 2001, ApJS, 134, 331
Fogle, M., Badnell, N. R., Glans, P., et al. 2005, A&A, 442, 757
Fritzsche, S., Surzhykov, A., & Volotka, A. 2015, NJPh, 17, 103009
Gu, M. F. 2003, ApJ, 590, 1131
Huang, Z. K., Wen, W. Q., Wang, H. B., et al. 2015, PhyS, T166, 014023
Huang, Z. K., Wen, W. Q., Xu, X., et al. 2017, NIMPB, 408, 135
Kallman, T., & Bautista, M. 2001, ApJS, 133, 221
Kallman, T. R., & Palmeri, P. 2007, RvMP, 79, 79
Kilgus, G., Habs, D., Schwalm, D., et al. 1992, PhRvA, 46, 5730
Kramida, A., Ralchenko, Y., Reader, J., & Team, N. A. 2015, http://physicsnistgov/asd
Landi, E., Doron, R., Feldman, U., & Doschek, G. A. 2001, ApJ, 556, 912
Lepson, J., Beiersdorfer, P., Behar, E., & Kahn, S. 2003, ApJ, 590, 604
Mazzotta, P., Mazzitelli, G., Colafrancesco, S., & Vittorio, N. 1998, A&AS, 133, 403
Meng, L.-J., Ma, X.-W., Parkhomchuk, V. V., et al. 2013, ChPhC, 37, 017004

Müller, A. 2008, in Advances In Atomicc, Molecular, and Optical Physics, ed. P. R. B. Ennio Arimondo & C. L. Chun (New York: Academic), 293
Orban, I., Böhm, S., Loch, S. D., & Schuch, R. 2008, A&A, 489, 829
Orban, I., Loch, S. D., Böhm, S., & Schuch, R. 2010, ApJ, 721, 1603
Orlov, D. A., Krantz, C., Bernhardt, D., et al. 2009, Journal of Physics: Conference Series, 163, 012058
Paerels, F. B. S., & Kahn, S. M. 2003, ARA&A, 41, 291
Romanik, C. J. 1988, ApJ, 330, 1022
Saloman, E. B. 2010, JPCRD, 39, 033101
Savin, D. W. 2007, Journal of Physics: Conference Series, 88, 012071
Savin, D. W., Gwinner, G., Grieser, M., et al. 2006, ApJ, 642, 1275
Schippers, S. 2012, Journal of Physics: Conference Series, 388, 012010
Schippers, S. 2015, NIMPB, 350, 61
Schippers, S., Bernhardt, D., Müller, A., et al. 2012, PhRvA, 85, 012513
Schippers, S., Müller, A., Gwinner, G., et al. 2001, ApJ, 555, 1027
Schippers, S., Schmidt, E. W., Bernhardt, D., et al. 2007, PhRvL, 98, 033001
Schippers, S., Schnell, M., Brandau, C., et al. 2004, A&A, 421, 1185
Schnell, M., Gwinner, G., Badnell, N. R., et al. 2003, PhRvL, 91, 043001
Schuch, R., & Böhm, S. 2007, Journal of Physics: Conference Series, 88, 012002
Shull, J. M., & Van Steenberg, M. 1982, ApJS, 48, 95
Träbert, E., Beiersdorfer, P., Utter, S., et al. 2000, ApJ, 541, 506
Wang, K., Guo, X. L., Liu, H. T., et al. 2015, ApJS, 218, 16
Wen, W. Q., Ma, X., Xu, W. Q., et al. 2013, NIMPB, 317, 731
Wu, J. X., Zang, Y. D., Nolden, F., et al. 2013, NIMPR, 317, 623 Part B
Zhao, H. W., Sun, L. T., Guo, J. W., et al. 2017, Physical Review Accelerators and Beams, 20, 094801